Theory of the birefringence due to dislocations in single crystal CVD diamond

2009 J. Phys.: Condens. Matter 21 364220

(http://iopscience.iop.org/0953-8984/21/36/364220)

J. Phys.: Condens. Matter **21** (2009) 364220 (7pp) doi:10.1088/0953-8984/21/36/364220

Theory of the birefringence due to dislocations in single crystal CVD diamond

H Pinto and R Jones

School of Physics, University of Exeter, Stocker Road, Exeter EX4 4QL, UK

E-mail: pinto@excc.ex.ac.uk

Received 4 April 2009, in final form 17 June 2009
Published 19 August 2009
Online at stacks.iop.org/JPhysCM/21/364220

Abstract

Single crystal diamond grown by chemical vapour deposition (CVD) often exhibits strain induced birefringence arising from bundles of edge dislocations lying almost parallel to the [001] growth axis. The birefringent pattern changes when the crossed-polarizers are rotated with respect to the underlying lattice. For polarizers parallel to ⟨110⟩ directions, the birefringence pattern consists of four bright petals with dark arms along ⟨110⟩. For polarizers parallel to ⟨100⟩, the birefringence pattern consists of eight petals of weaker intensity with dark arms along ⟨110⟩ and ⟨100⟩ directions. We evaluate the birefringence intensity by using isotropic elasticity theory and find that these patterns can be explained by a specific dislocation arrangement which is consistent with x-ray topographic studies.

(Some figures in this article are in colour only in the electronic version)

1. Introduction

Homoepitaxially deposited single crystal diamond can be grown remarkably free from unwanted impurities and defects by chemical vapour deposition (CVD). However, in spite of the favourable conditions of growth, edge and mixed dislocations of density about $\sim 10^5$ cm^{-2}, lying approximately along the [001] growth direction, are a source of concern [1]. These dislocations act as non-radiative recombination centres [2]. Previous investigations show that they can be decorated with nitrogen impurities [3] and their atomistic structure has been modelled using density functional theory [4, 5]. These dislocations often appear in bundles lying almost parallel to the [001] growth axis and fan out along ⟨110⟩. Detailed studies using x-ray topography show that, in many cases, the dislocations are observed in groups of four or more lines diverging from a defect on or near the substrate. Where only four lines are observed to emanate from a given point, the dislocations deviate from [001] in such a way that their projections onto the (001) plane lie along ⟨110⟩ directions. Often, those with projections along [110] or [$\bar{1}\bar{1}$0] have [1$\bar{1}$0] Burgers vectors, and those with projections along [1$\bar{1}$0] or [$\bar{1}$10] have [110] Burgers vectors. These dislocations are predominantly edge type dislocations [6].

Diamonds containing such bundles exhibit a birefringence with a few strikingly bright regions with a characteristic pattern consisting of four approximately equally bright petals as shown in figure 1. There is a close connection between these four-petalled defects and dislocations. X-ray topographs reveal that the regions where the defects are seen coincide with dense bundles of dislocations [6]. This suggests that in this case the birefringence is not due to inclusions.

Figure 1. Birefringence seen in crossed-polarizers of two four-petalled defects in CVD diamond. The plane of view is (001). The horizontal and vertical axes lie along ⟨100⟩ and the polarizers lie along ⟨110⟩. Figure provided by Martineau.

The four-petalled pattern shown in figure 1 is not invariant under a rotation of the crystal about [001], i.e. the pattern changes with the directions of the crossed-polarizers (figure 2).

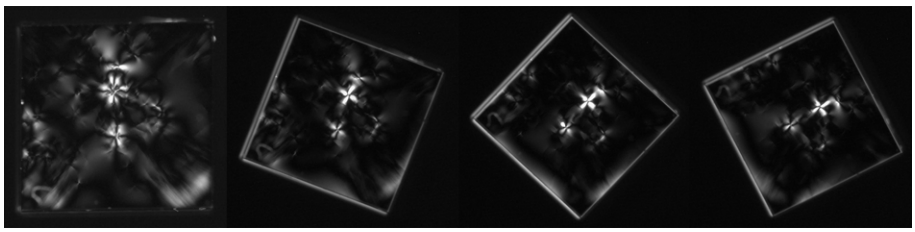

Figure 2. Birefringence of a petalled defect when the crystal is rotated with respect to the cross-polarizers by 0°, 22°, 45° and 67° from ⟨100⟩. Note that eight dark arms are seen when a polarizer is parallel to ⟨100⟩ and four dark lobes in other cases. Exposure times are 1.9, 0.5, 0.23 and 0.37 s revealing a weaker birefringence in the case when the polarizers are along ⟨100⟩. Figure provided by Martineau.

Thus the strain field is linked to the underlying crystallography as expected from a dislocation model. This is not the case for a spherical inclusion which also gives a four-petal pattern with dark arms along the polarizer directions but would not rotate with the crystal. The lobes seen when the polarizers are parallel to ⟨100⟩ are weaker than the bright lobes seen for the case when the polarizers lie along ⟨110⟩.

The spatial extent of the birefringence in the (001) plane is about 13% of the crystal size or about 300–400 μm, given that the crystal is about 3 mm in size. Clearly, the birefringence of a single dislocation does not extend over this distance, and the resultant strain due to a bundle of many dislocations must be considered.

We note that the dislocations arise only in the epilayer and not the underlying substrate. Since dislocations cannot terminate within the crystal, the bundle must be composed of dislocation dipoles with zero net Burgers vector [7]. The effect of the divergence in dislocation line directions, clearly seen in the x-ray topographic experiments, must be included in order to assess the spatial extent of the birefringence, and we show that the four-petalled pattern can arise from a compact defect on the substrate surface with dimensions less than a few micrometres. It is the aim of this paper to discuss possible arrangements of dislocations that give rise to the strain maps and birefringence patterns observed. This is done by finding the strain fields and birefringence of bundles of dislocations and comparing them with experiment.

2. Birefringence of a single edge dislocation

The strain field of a bundle of dislocations can be found using isotropic elasticity theory by summing the strains due to individual edge dislocations. The principal values of the strain tensor and their directions are then calculated. The phase difference between the two polarized components of the light ray at the exit of the crystal is

$$\delta = 2\pi(n_1 - n_2)t/\lambda, \tag{1}$$

where n_1 and n_2 are the refractive indices of the crystal along the principal directions of strain, λ is the wavelength (550 nm) and t is the optical thickness of the crystal taken to be 2.52 mm. The refractive indices are related to the strain through the strain-optic coefficients p_{ij}. For stressed cubic materials

$$n_1 - n_2 = -n^3(p_{11} - p_{12})(\epsilon'_{11} - \epsilon'_{22})/2, \tag{2}$$

where ϵ'_{ii} are the principal values of the strain tensor and n is the refractive index of diamond. The experimental values of the strain-optic coefficients of diamond have been recently reviewed [8], and we have previously calculated $p_{11} - p_{12}$ to be -0.3 [9]. This is close to the experimental value. Thus light polarized along the principal direction associated with ϵ'_{11} moves with the slower speed if $\epsilon'_{11} > \epsilon'_{22}$. This direction corresponds with tensile strain. We note that δ is simply related to the shear strain $(\epsilon'_{11} - \epsilon'_{22})/2$ and hence a map of δ gives the shear strain field in the (001) plane. The intensity of birefringence is given by $I = E^2 \sin^2(2\phi) \sin^2(\delta/2)$ where ϕ is angle between a principal axis of strain and a polarizer [10]. To avoid confusion we define the normalized birefringence as $\sin^2(2\phi) \sin^2(\delta/2)$.

For an edge dislocation lying along z, with the Burgers vector of magnitude b, taken to be $a/\sqrt{2}$, and parallel to x, the strain tensor ϵ_{ij} and its principal values ϵ'_{ii} are well known and lead to a shear strain of [11]

$$\begin{aligned} \epsilon'_{11} - \epsilon'_{22} &= -2Ax/r^2, \\ \theta &= \tfrac{1}{2}\tan^{-1}\{(y^2 - x^2)/(2xy)\}. \end{aligned} \tag{3}$$

Here $A = b/(4\pi(1-\nu))$, ν is Poisson's ratio, $r^2 = x^2 + y^2$ and θ is the angle between the Burgers vector and a principal direction of strain. We note that $n_1 - n_2$ decreases with distance from the core as $1/r$.

The strain field, proportional to δ, and birefringence of a single edge dislocation with Burgers vector along [100] are shown in figure 3 for the cases when the polarizer is along [100] and [110]. The birefringence reveals a characteristic dipole pattern which turns into a four-petalled pattern when the crossed-polarizers are turned through 45°. The patterns can be simply understood from the principal strains and their directions given above. We note that the intensity vanishes when either $\delta = 0$ or a principal axis is parallel to a polarizer. Equations (1)–(3) show that the former is the case along the y-axis while the latter occurs along the x-axis and when the polarizer lies 45° to the x-axis. This is because a principal axis of strain is then parallel to the polarizer. Thus the great change in the birefringence when the polarizer is rotated by 45° seen in figure 3 can easily be seen to arise from the strain field of the edge dislocation. We note, however, that the birefringence is quite different from the experimental one shown in figure 2. In summary, the shear strain map and birefringence of a single edge dislocation cannot describe the four-petalled defect and alternative models must be considered.

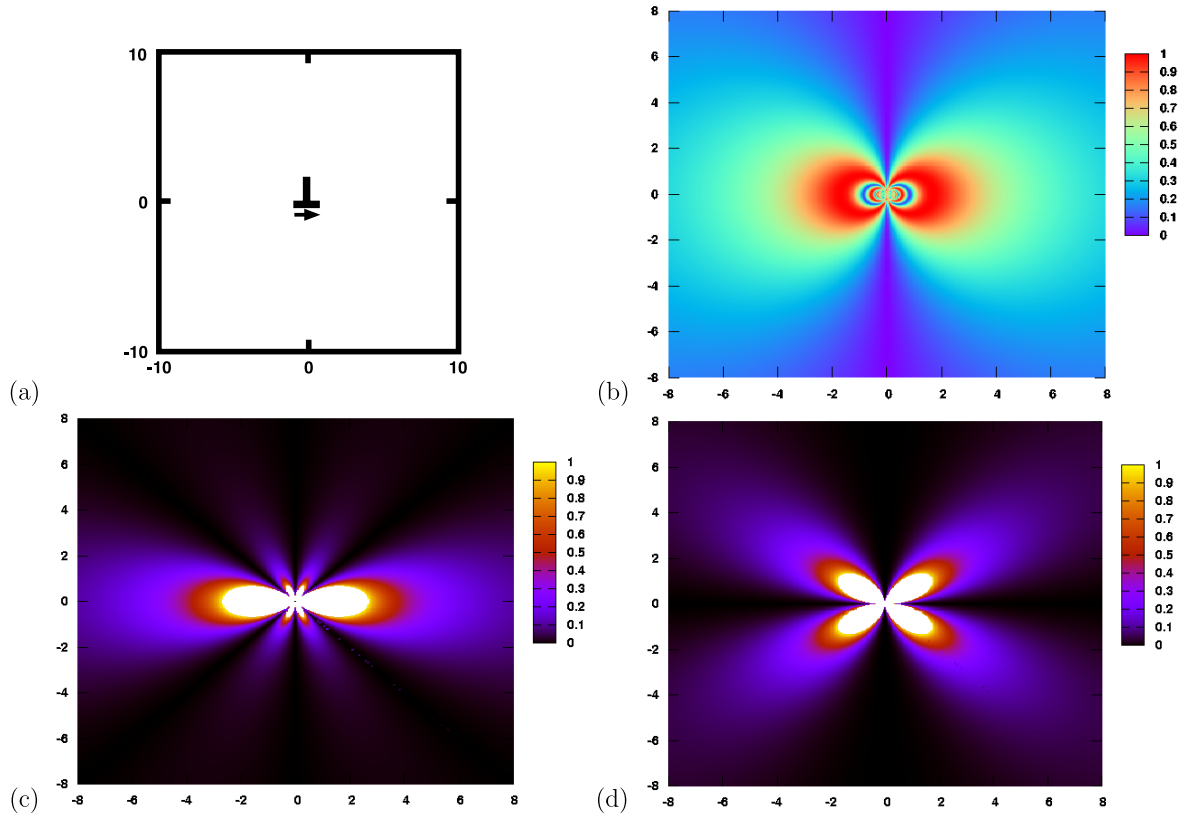

Figure 3. (a) Projection of edge dislocation line lying along [001] onto (001). The Burgers vector is indicated by the arrow. (b) Map of $|\sin\delta|$ which is proportional to the shear strain. (c), (d) Normalized birefringence map in the (001) plane when a crossed-polarizer lies along x and at 45° to x. Note the dipole character in (c) and four-petalled form in (d). Dark arms lie along y for both cases. The horizontal and vertical axes are in micrometres.

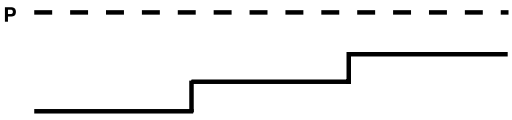

Figure 4. A kinked dislocation lying along [001] leads to the dislocation lying on average at an angle χ to the growth [001] axis, represented here as along the horizontal direction, in the ⟨110⟩ plane. The dashed line through P denotes a light ray.

3. Effect of line direction

We now consider the effect of the dislocation lines fanning out, or diverging as in a cone. The x-ray topographic results [6] show that the dislocations lie at an angle of about $\chi = 3°$–$5°$ with [001]. Such a divergence is expected to lead to a strain field at the top surface extending over $t/\tan\chi$ or ∼150 μm, where t is the thickness of the epilayer (2.52 mm), if the dislocations emerged from a point source near the substrate. The number of dislocations in the bundle has, however, to be chosen carefully to obtain agreement with the observed magnitude of δ.

To take into account the line direction we use an abrupt kink model as shown in figure 4 where a relatively few kinks are equally spaced along the dislocation line leading to a line direction of χ off [001]. Consider light passing along P (figure 4) parallel to [001]. If the Burgers vector is normal to the paper then, for all segments along the dislocation line, the birefringence intensity is zero as $\delta = 0$ at all points along the light direction. Consequently, the dark arms are not affected by the fanning out of the dislocations. Similarly, if the Burgers vector lies in the plane of the paper, then δ is not zero at P, and its magnitude depends on the distance of P from the dislocation line in the (001) plane. At large distances, when δ is small and much less than $\pi/2$, the effective δ for the kinked dislocation line is an average over all the values of δ for the individual segments. Thus this arm would remain bright as it is for an unkinked dislocation lying along [001]. Thus we conclude that the line direction of the dislocations does not alter our conclusions derived from [001] dislocations. Moreover, it suggests that we can take into account the divergence of the dislocations by evaluating the average strain tensor

$$\frac{1}{t}\int_0^t \mathrm{d}z\, \epsilon_{ij}(x, y, z), \tag{4}$$

where the strain is due to a dislocation lying at an angle χ with respect to the [001] growth direction.

4. The four-arm defect

The x-ray topographic results show that the petalled defect is associated with groups of edge dislocations emanating from

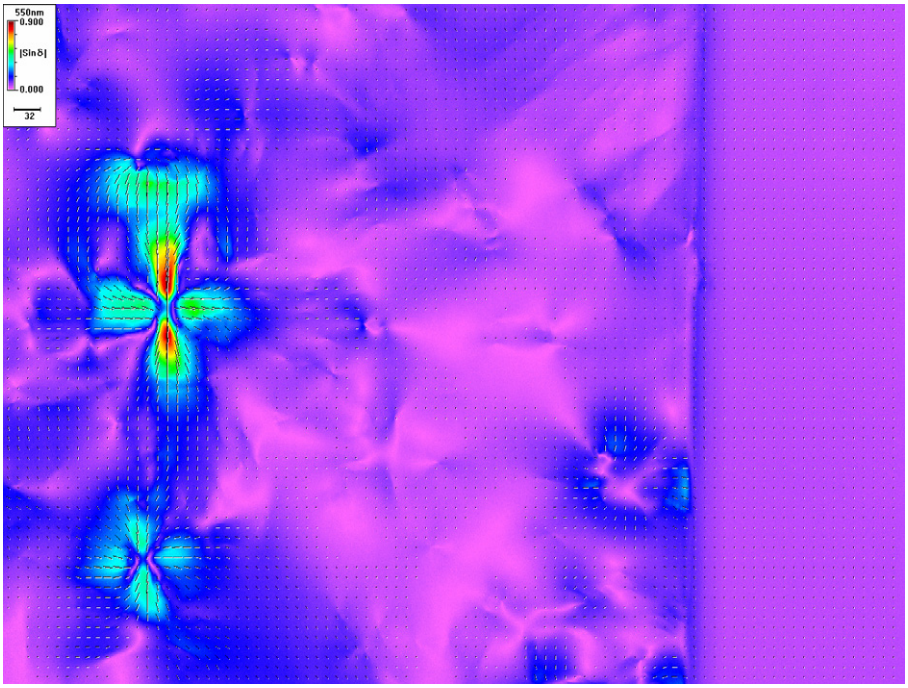

Figure 5. Phase difference $|\sin(\delta)|$ between the two polarized waves at the exit of the specimen of thickness 2.52 mm showing the four-petalled defect. The dashed lines parallel to the [100] and [010] edges of the specimen indicate the principal directions of strain for the slow direction of light propagation. Note that for points along [100] or [010] near the core, the directions of the slow axis are also parallel to these directions. Figure provided by Martineau.

a defect on or near the substrate surface and fanning out along ⟨110⟩ directions. Many of these dislocations have [110] Burgers vectors and lie about 3°–5° off [001] in the (110) plane, while those with $[01\bar{1}]$ Burgers vectors lie at a similar angle to [001] but in the $(01\bar{1})$ plane [6]. Here we shall investigate the strain field of the simplest arrangement having this structure consisting of a linear array of dislocations in each quadrant. We note that this arrangement has a four-fold rotational axis and such a symmetry is necessary to explain the strain field of the four-petalled defect shown in the lower part of figure 5. The other four-petalled defect lying in the upper part of figure 5 possesses a two-fold rotational symmetric strain field and will be discussed below.

We place 20 edge dislocations in the first quadrant all lying along $[\sin\chi, \sin\chi, \cos\chi]$ and intersecting the (001) plane at equidistant points along [110] as indicated schematically in figure 6(a). The dislocations all have the same $a/2[1\bar{1}0]$ Burgers vector. The separation of individual dislocations in each arm is 0.14 μm. Dislocations in the other three quadrants are found by rotating those in the first quadrant.

The dislocations introduce additional half-planes outside the core of the defect, which produce a net compression along the tangential direction and a radial tensile field. This is necessary to reproduce the radial slow axis shown in figure 5.

Figure 6 shows the calculated strain field and birefringence. The strain map reveals a four-petalled pattern with dark arms corresponding to zero shear strain along ⟨110⟩, as is indeed observed. Since δ is zero along the four ⟨110⟩ directions, it follows that the birefringence vanishes along these directions for all directions of the polarizer. This accounts for the four-fold pattern seen in birefringence for polarizers lying other than along ⟨100⟩. For points along say [100], we find that the principal axes of strain also lie along ⟨100⟩ directions and in fact the tensile axis lies along this [100]. This is also in agreement with the experiment as shown in figure 5.

Consider now the birefringence for the polarizers lying along ⟨100⟩. In this case, the four ⟨100⟩ directions are also dark as these directions coincide with the principal axes of strain. Figure 6 shows the birefringence map for this case and we find eight arms, in agreement with observation. The long exposure time required to reveal this structure is also in agreement with the theory, as shown when figures 2 and 6 are compared. Finally, we note that the extent of the birefringence, which is proportional to the number of dislocations, is around 300–400 μm and consistent with the observations. At 400 μm along [100], the principal strains are 1.53×10^{-6} and -1.26×10^{-6}. These are equivalent to stresses of about 3 MPa.

5. Superposition of bundles of dislocations

It is to be noted that the strain field of some of the observed four-petal defects have a pair of opposite lobes of greater brightness than the other pair. This is clearly seen for the defect in the upper part of figure 5. We now introduce a model which displays such an asymmetry. It is clear that these defects possess additional sources of strain lying along one of the ⟨100⟩ directions.

We first investigate a two-arm defect having a linear array of edge dislocations lying along [010] with Burgers vector along [100], and a second linear array along $[0\bar{1}0]$ with Burgers vector along $[\bar{1}00]$. The projection of the dislocations in each

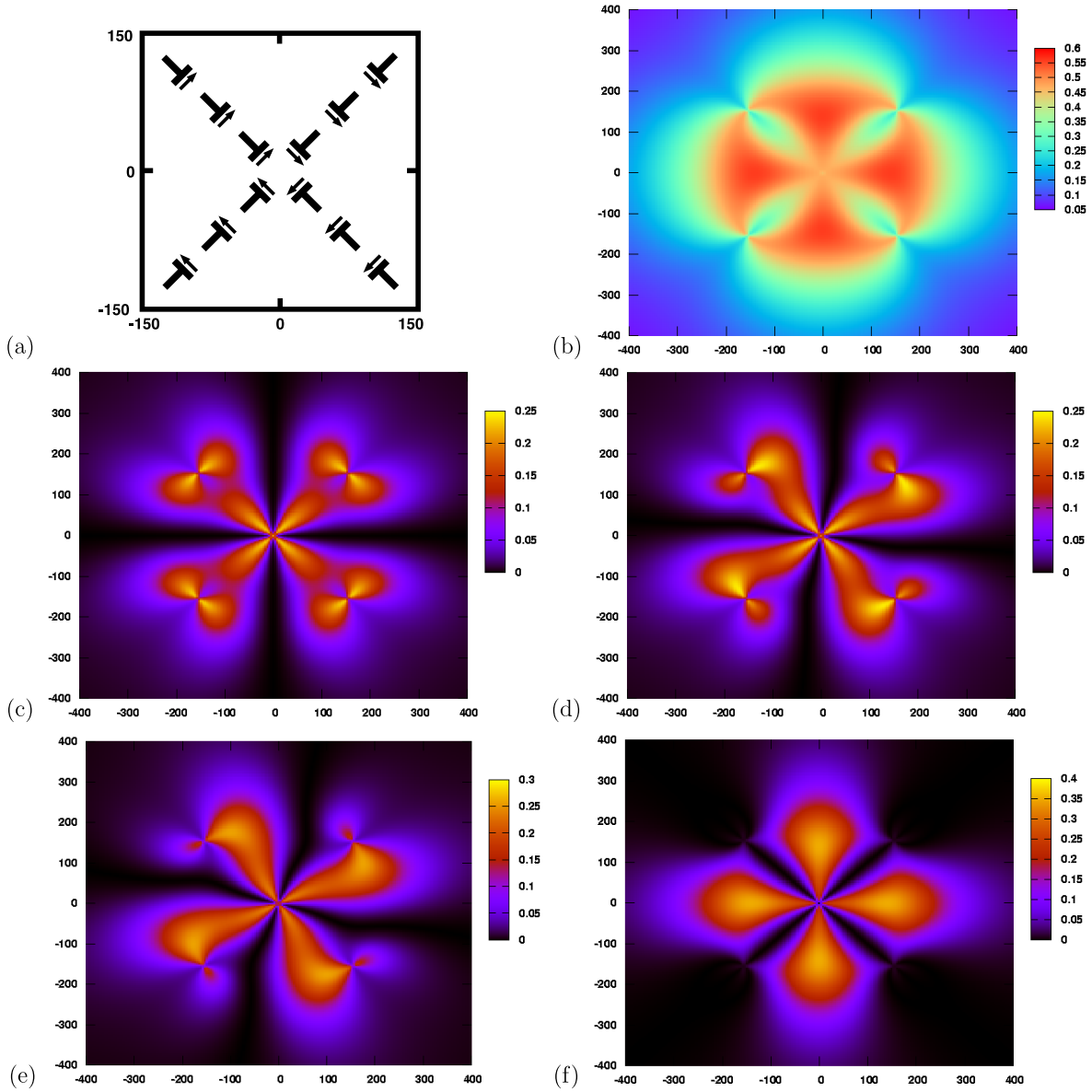

Figure 6. The calculated strain field and birefringence of the four-arm defect where each arm contains 20 dislocations with separation 0.14 Å. (a) Projection of dislocation lines onto (001). The Burgers vectors of the edge dislocations in each arm are indicated by the arrows. The dislocations are inclined 3.5° to [001] and the thickness of the crystal is 2.52 mm. The projection reveals the four-fold symmetry of the bundle. (b) Map of $|\sin\delta|$ or shear strain of the bundle. Note the presence of four bright lobes along ⟨100⟩ in agreement with observations shown in figure 5. (c)–(f) Normalized birefringence for polarizers at angles of 0°, 15°, 30° and 45° to [100]. Note the extent of the birefringence is about 300 μm and that there is a weaker birefringence when the polarizers are parallel to [100] than at an angle of 45° with [100]. The birefringence shows eight bright lobes in the first case and four in the second.

arm onto the (001) plane is schematically shown in figure 7. It might seem surprising that we are assuming the Burgers vectors to lie along ⟨100⟩ rather than ⟨110⟩ but we note that the strain field of each dislocation with Burgers vector a [100] is the sum of the strains of two dislocations with the Burgers vectors a [110]/2 and a [1$\bar{1}$0]/2. In other words, a pair of arms in the four-arm defect have been pulled towards each other until they lie along ⟨100⟩.

Figure 7 also shows the resulting strain field to be dipolar with dark arms along [010]. The birefringence has four lobes and six lobes of differing intensities when the polarizers are respectively parallel to [100] and [110].

It should be noted that the strain map can be easily understood from the strain map of a single dislocation shown in figure 3. However, even though the strain maps are similar, the birefringence is not. In the case when a polarizer lies along [100], two bright lobes are found for the single dislocation but four bright lobes are found for the two-arm defect described here. This is because a principal axis of strain lies along [100] as a consequence of the two-fold symmetry present in the two-arm defect. This then makes this direction dark in birefringence when the polarizer lies along [100].

The bright lobes along [100], and the dark arms along [010] for the strain field in the four-arm defect suggests that

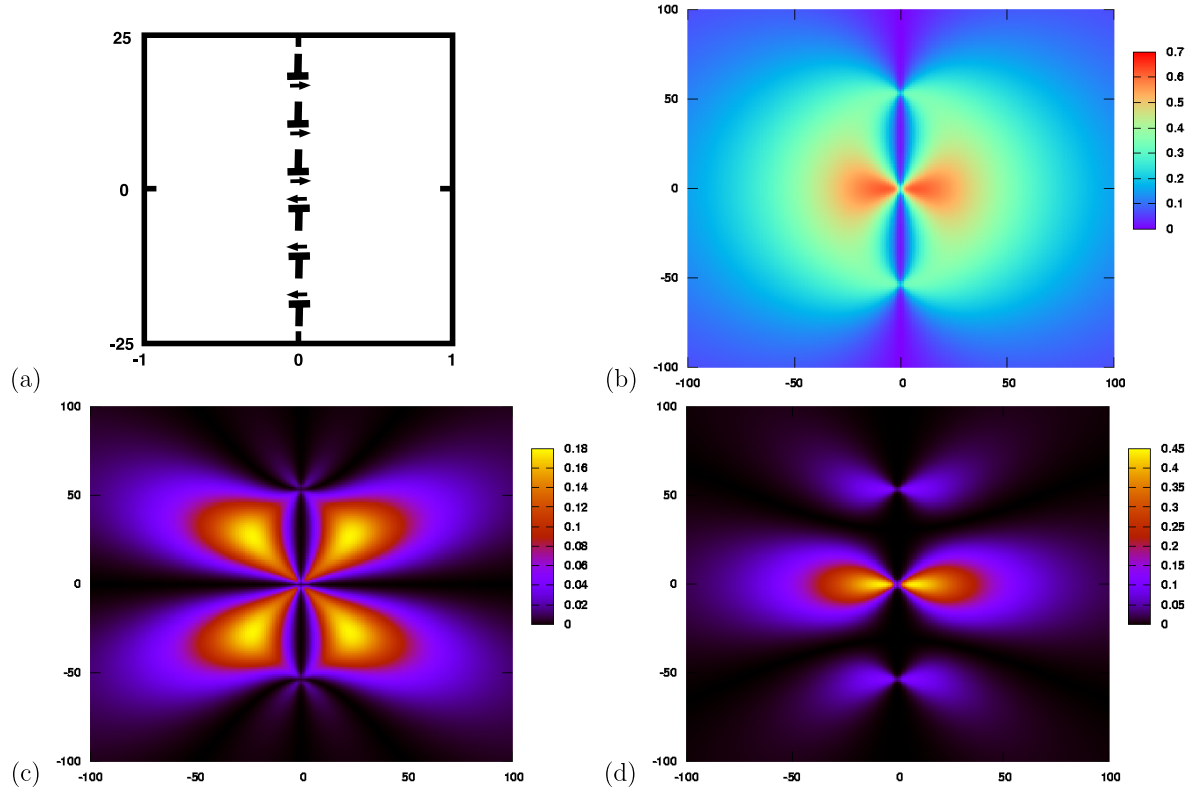

Figure 7. (a) (001) Projection of edge dislocations lying in two arms along [010]. The 20 dislocations lying along $[0, \sin\chi, \cos\chi]$ with χ equal to 3.5°, in the top arm all have separation of 0.1 μm and Burgers vectors along [100]. The dislocations in the bottom arm lie along $[0, -\sin\chi, \cos\chi]$ and have the same Burgers vector of $[\bar{1}00]$. (b) Map of $|\sin\delta|$ of the two-arm defect showing a dipole along [100] and a dark arm along [010]. (c), (d) Normalized birefringence of the two-arm defect for polarizers parallel to $\langle 100\rangle$ and $\langle 110\rangle$, respectively. In this case, four dark lobes lie along $\langle 100\rangle$ when the polarizers are parallel to $\langle 100\rangle$ and the birefringence exhibits two bright lobes along $\langle 100\rangle$ when the polarizers are parallel to $\langle 110\rangle$.

the strain map of this defect, when added to the strain field of the four-arm defect, would possess four bright lobes along both [100] and [010] but the intensity along [100] would exceed that along [010]. Figure 8 shows this is the case. To obtain the observed intensity pattern, we chose three times as many dislocations in the four-arm bundle as in the two-arm. If this ratio is increased, then the four bright lobes become equally bright, and if the ratio was decreased then the strain map approached two lobes as shown in figure 7. The birefringence shown in figure 8 has a symmetrical set of four or eight lobes for a polarizer along $\langle 100\rangle$ but the four lobes seen when the polarizer lies along $\langle 110\rangle$ have different intensities.

6. Discussion

We have analysed the strain field and birefringence of several linear arrays of dislocations which could be responsible for a number of petalled defects seen in single crystal homoepitaxially grown CVD diamonds. These defects are associated with arrays of threading (001) dislocations with edge character. The strain field of a single edge dislocation as well as its birefringence cannot explain the magnitude of the birefringence associated with the four-petalled defect. Moreover, if the net Burgers vector of the defect is non-zero, then asymptotically, its strain field must be dipole like and in conflict with the observed strain field of the four-petalled defect. Thus the defect must be composed of dislocation dipoles.

The birefringence of four linear arrays of edge dislocations located on four arms lying along $\langle 110\rangle$ directions with $\langle \bar{1}10\rangle$ Burgers vectors leads to a strain field with four bright petals along $\langle 100\rangle$ as observed. The birefringence associated with the defect is sensitive to the directions of the polarizers. If these are along $\langle 110\rangle$, then four bright lobes are also seen along $\langle 100\rangle$. If the polarizers are parallel to $\langle 100\rangle$, then eight weak lobes are seen. Such patterns reflect the four-fold symmetry of the defect. With the arrangement of dislocations and Burgers vectors shown in figure 6, with the extra half-planes of atoms in each dislocation lying outside the core, the principal axis of strain associated with the slower polarized ray is radial, as observed. The birefringence is seen to extend to about 400 μm and this requires about 20 dislocations in each arm or 80 dislocations in the bundle. The shear strain, averaged over the epilayer thickness, introduced by these dislocation arrays and 400 μm along the cube axes is about 10^{-6}, leading to a stress of about 3 MPa which decays slowly as $1/r$ where r is the distance to the core.

It is, however, to be noted that not all experimental strain images have perfect four-fold symmetry. They often have one pair of opposite lobes brighter than the other pair. Such patterns could be due to the more complex arrangements shown in

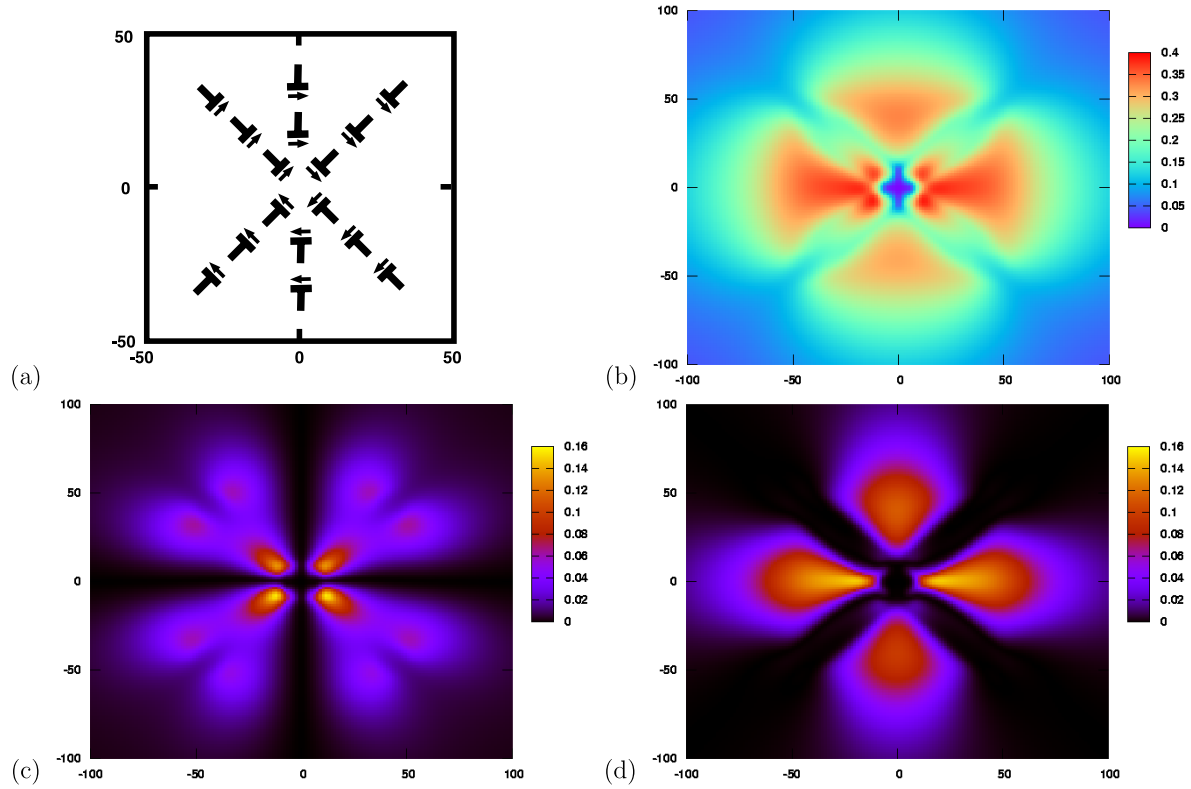

Figure 8. Superposition of four-arm and two-arm defects. (a) Projection onto (001) of the six arms of the resulting arrangement. See text. Eight dislocations lie along [010] and twelve along each of the ⟨110⟩ directions. The thickness of the crystal is 0.83 mm and χ is 3°. (b) The strain field of the resulting bundle showing four lobes but two lying along [100] are brighter than the other pair. (c), (d) The normalized birefringence for polarizers parallel to ⟨100⟩ and ⟨110⟩, respectively. These show four or eight lobes with dark arms along ⟨100⟩ for the former, and four bright lobes along ⟨100⟩, with differing intensities, for the latter. The birefringence is weaker in (c) than in (d).

figure 8. The model of the arrays of dislocations, in particular the four-fold symmetry, has implications for the structure of the defect, possibly lying on the substrate, which acts as a source for the dislocations.

Acknowledgments

We thank Philip Martineau and Mike Gaukroger for extensive discussions and experimental data. We also thank De Beers UK and EPSRC for financial support.

References

[1] Martineau P M, Lawson S C, Taylor A J, Quinn S J, Evans D J F and Crowder M J 2004 *Gems Gemol.* **40** 2
[2] Martineau P, Gaukroger M, Khan R and Evans D, unpublished
[3] Mora A E, Steeds J W, Butler J E, Yan C-S, Mao H K, Hemley R J and Fisher D 2005 *Phys. Status Solidi* a **202** 2943
[4] Fujita N, Blumenau A T, Jones R, Oberg S and Briddon P R 2006 *Phys. Status Solidi* a **203** 3070
[5] Fujita N, Blumenau A T, Jones R, Oberg S and Briddon P R 2007 *Phys. Status Solidi* a **204** 2211
[6] Gaukroger M P, Martineau P M, Crowder M J, Friel I, Williams S D and Twitchen D J 2008 *Diamond Relat. Mater.* **17** 262
[7] Klapper H 2000 *Mater. Chem. Phys.* **66** 101
[8] *Proc. Diamond Conf.* 2007
[9] Hounsome L S, Jones R, Shaw M J and Briddon P R 2006 *Phys. Status Solidi* a **203** 3088
[10] Born M and Wolf E 2001 *Principles of Optics* 7th edn (Cambridge: Cambridge University Press) p 824
[11] Bullough R 1957 *Phys. Rev.* B **110** 620